# Sensitivity of Spin-Precession Axion Experiments

Jeff A. Dror and Stefania Gori
*Department of Physics, University of California Santa Cruz, 1156 High St., Santa Cruz, California 95064, USA and Santa Cruz Institute for Particle Physics, 1156 High St., Santa Cruz, California 95064, USA*

Jacob M. Leedom
*Deutsches Elektronen-Synchrotron DESY, Notkestrasse 85, 22607 Hamburg, Germany*

Nicholas L. Rodd
*Theoretical Physics Department, CERN, 1 Esplanade des Particules, CH-1211 Geneva 23, Switzerland*

(Received 25 October 2022; accepted 17 March 2023; published 1 May 2023)

We study the signal and background that arise in nuclear magnetic resonance searches for axion dark matter, finding key differences with the existing literature. We find that spin-precession instruments are much more sensitive than what has been previously estimated in a sizable range of axion masses, with sensitivity improvement of up to a factor of 100 using a $^{129}$Xe sample. This improves the detection prospects for the QCD axion, and we estimate the experimental requirements to reach this motivated target. Our results apply to both the axion electric and magnetic dipole moment operators.

DOI: 10.1103/PhysRevLett.130.181801

The axion, a light scalar whose leading interactions exhibit a shift symmetry, is one of the most compelling extensions to the standard model of particle physics. Originally proposed as an elegant solution to the strong $CP$ problem [1–4], axions have since been appreciated for both their ubiquity in string theory [5–7] and the generic expectation that they contribute to cold dark matter through, for example, misalignment production [8–10]. The continuous shift symmetry of the axion leads to a natural expectation that the axion should be an extraordinarily light state, with mass $m_a \ll 1$ eV suppressed by its decay constant $f_a$, which arises from breaking the continuous symmetry to a discrete one via instanton effects. Such a small mass implies that axion dark matter on Earth should be well described by a classical wave.

At low energies, the possible interactions of an axion, $a$, with a nucleon $N$ take the following form:

$$\mathcal{L} \supset g_N(\partial_\mu a)\bar{N}\gamma^\mu\gamma_5 N - \frac{i}{2} g_d a \bar{N}\sigma_{\mu\nu}\gamma_5 N F^{\mu\nu}. \tag{1}$$

In the presence of an axion-wave background, these interactions source an oscillating magnetic dipole (MD), weighted by $g_N \propto 1/f_a$, and an oscillating electric dipole (ED), weighted by $g_d \propto 1/m_N f_a$, with $m_N$ the nucleon mass. For the QCD axion, $g_N$ depends on the charge assignments and field content of the UV theory, whereas $g_d$ depends on the term that resolves the strong $CP$ problem, $(a/f_a)G^{\mu\nu}\tilde{G}_{\mu\nu}$, and is fixed to $g_d = (3.7 \pm 1.5) \times 10^{-18}\ \mathrm{GeV}^{-2}(10^{15}\ \mathrm{GeV}/f_a)$ [11]. For a nonrelativistic nucleus, these interactions lead to the Hamiltonian, $H_{\mathrm{int}} = -2(g_N\nabla a + g_d a\mathbf{E}^*)\cdot\mathbf{S}$. Here, $\mathbf{S}$ is the nucleon spin operator, and $\mathbf{E}^*$ is the effective electric field felt by a nucleus (and differs from the applied field by at least 2 orders of magnitude due to shielding by the atomic electrons). By drawing an analogy between the interaction of spins and a magnetic field, the axion-nucleus interaction can be characterized as an effective axion magnetic field,

$$\mathbf{B}_a(t) = -\frac{2}{\gamma}\begin{cases} g_N\nabla a(t) & \text{(MD)}, \\ g_d\mathbf{E}^* a(t) & \text{(ED)}, \end{cases} \tag{2}$$

with $\gamma$ being the gyromagnetic ratio of the nucleon. This axion-induced magnetic field can be detected using spin-precession techniques such as nuclear magnetic resonance (NMR), as originally proposed in the seminal CASPEr papers [12,13], and it was further developed experimentally and theoretically in Refs. [14–23]. The CASPEr approach is opening up a frontier for axion dark-matter direct detection beyond the widely exploited axion-photon coupling (for related proposals, see Refs. [24–44]).

In this Letter, we revisit the sensitivity of spin-precession experiments, clarifying fundamental aspects of the behavior of the expected axion signal and noise sources. The system depends on three fundamental timescales: the axion coherence time, $\tau_a \sim (4\ \mathrm{neV}/m_a)$ sec, the transverse

spin-relaxation time, $T_2$, and the experimental integration time, $T$. We demonstrate that there are two previously overlooked effects that enhance the growth of the signal when $\tau_a < T_2$, a realization that improves the prospects for QCD axion detection with spin-precession instruments, and we comment on the requirements to achieve this goal. We further reconsider a dominant noise source—spin-projection noise—and demonstrate that it is larger at high axion masses, thereby reducing the utility of using materials with large magnetic moments.

*The NMR axion signal.*—We begin with a brief review of spin-precession axion experiments. Fundamentally, they involve a macroscopic sample of atoms with nonzero nuclear spin placed within a static magnetic field, $\mathbf{B}_0$. The field induces a bulk magnetization $\mathbf{M}_0$ that is parallel to $\mathbf{B}_0$. A perpendicular magnetic field—such as that induced by the axion—will rotate the nuclear spins by a small amount. However, as soon as they do, the spins will precess around $\mathbf{B}_0$ at the Larmor frequency, $\omega_0 \equiv \gamma B_0$, generating an oscillating transverse magnetization, which can then be detected with a sensitive magnetometer. For $m_a \sim \omega_0$, the effect is resonantly enhanced, with the width of the system's response controlled by the transverse relaxation time, $T_2$, which is a macroscopic property of the sample and quantifies how long the precession of the transverse spins can be maintained coherently. By varying $\mathbf{B}_0$, the instrument can scan a range of axion masses.

To study the dynamics of the magnetization, we turn to the Bloch equations. Preparing the sample with $\mathbf{M}_0 \propto \mathbf{B}_0 \propto \hat{\mathbf{z}}$, the Bloch equations read

$$\frac{d\mathbf{M}}{dt} = \mathbf{M} \times \gamma \mathbf{B} - \frac{M_x \hat{\mathbf{x}} + M_y \hat{\mathbf{y}}}{T_2} - \frac{(M_z - M_0)\hat{\mathbf{z}}}{T_1}. \quad (3)$$

The longitudinal relaxation time commonly satisfies $T_1 \gg T_2$, and we will work in the limit where $T_1$ is much longer than any other timescale of interest, so that it will play no further role in our discussion. We decompose the magnetic field as $\mathbf{B} = B_0 \hat{\mathbf{z}} + \mathbf{B}_a(t)$. As $|\mathbf{B}_a(t)| \ll B_0$, we study the magnetization perturbatively, taking $\mathbf{M} \simeq \mathbf{M}_0 + \mathbf{M}_a$, and we will work only to linear order in the axion-induced fields throughout [45]. Working to this order, $M_z(t) = M_0$, leaving the dynamics to the transverse magnetizations,

$$\begin{aligned} \dot{M}_x &= \omega_0 M_y - T_2^{-1} M_x - M_0 \gamma B_{ay}, \\ \dot{M}_y &= -\omega_0 M_x - T_2^{-1} M_y + M_0 \gamma B_{ax}. \end{aligned} \quad (4)$$

These equations can be decoupled. If we measure the $\hat{\mathbf{x}}$ component of the magnetization, the equation to solve is

$$\begin{aligned} &\ddot{M}_x + 2T_2^{-1}\dot{M}_x + \omega_0^2 M_x \simeq F(t), \\ &\text{where, } F(t) = \gamma M_0 [\omega_0 B_{ax} - \dot{B}_{ay}]. \end{aligned} \quad (5)$$

Here and throughout, we neglect terms of $\mathcal{O}(1/\omega_0 T_2)$, as they are significantly suppressed. Equation (5) has reduced the system to the form of a simple harmonic oscillator with a resonant frequency $\omega_0$ and bandwidth $1/T_2$, that is being driven by the axion wave. Assuming $M_x(0) = M_y(0) = 0$, the solution is given by [46]

$$M_x(t) = \frac{1}{\omega_0} \int_0^t dt'\, e^{(t'-t)/T_2} \sin[\omega_0 (t - t')] F(t'). \quad (6)$$

To complete our solution for the magnetization, we require a model for the axion field. Here we treat the axion as a field with a fluctuating phase—we show that our results are reproduced when the axion is modeled as a sum over plane waves in [47]. The axion is taken to have constant amplitude $a_0 = \sqrt{2\rho_{\rm DM}}/m_a$, fixed by the local dark-matter density, and oscillates with frequency $\omega_a \simeq m_a(1 + v^2/2)$. The statistics of the field are then encoded by requiring the field, which carries velocity $v \sim 10^{-3}$, obtain a new random phase uniformly sampled on $[0, 2\pi)$, every coherence time, $\tau_a = 2\pi/m_a v^2$ [48]. Each time the phase is updated, we further update the direction of the axion field's momentum, $\mathbf{k}$ (where $|\mathbf{k}| = m_a v$), though, parametrically, our results are insensitive to the stochastic nature of the momentum vector. In summary,

$$\begin{aligned} F(t) &= A \cos[\omega_a t + \varphi(t)], \\ A &\equiv 2 M_0 a_0 \begin{cases} g_N \sqrt{\omega_0^2 (\mathbf{k} \cdot \hat{\mathbf{x}})^2 + \omega_a^2 (\mathbf{k} \cdot \hat{\mathbf{y}})^2}, \\ g_d \omega_0 E^*, \end{cases} \end{aligned} \quad (7)$$

where we focus on the dominant term in the driving force, which carries a phase $\varphi(t)$, uniformly sampled on $[0, 2\pi)$, but shifted from the axion phase. Furthermore, we assumed $\mathbf{E}^* \propto \hat{\mathbf{x}}$ for the ED operator. From Eq. (5), a resonant response is induced in the system when $|\omega_0 - \omega_a| \lesssim \pi \max[\tau_a^{-1}, T_2^{-1}]$. We will assume a scan strategy such that this condition is always satisfied, and thereby assume $\omega_a \simeq \omega_0$.

Whenever $t \ll \tau_a$, the axion behaves as if it were a perfectly coherent driving force: $\varphi$ and $\mathbf{k}$ are constant, so that Eq. (6) yields the following oscillating solution

$$M_x(t) \simeq (1 - e^{-t/T_2}) \frac{A T_2}{2\omega_0} \sin[\omega_0 t + \varphi]. \quad (8)$$

For $t \ll T_2$, the amplitude grows linearly in time. Beyond $T_2$, however, the growth saturates.

We next extend these results to finite $\tau_a$. Because of the stochastic variation of $\varphi$ and $\mathbf{k}$ for $t > \tau_a$, it is useful to compute the autocorrelation function of the induced magnetization, $C(t, t') \equiv \langle M_x(t) M_x(t') \rangle$,

$$\begin{aligned} C(t, t') = \frac{1}{\omega_0^2} \int_0^t d\bar{t} \int_0^{t'} d\bar{t}'\, e^{-(t-\bar{t})/T_2} e^{-(t'-\bar{t}')/T_2} \\ \times \sin[\omega_0 (t - \bar{t})] \sin[\omega_0 (t' - \bar{t}')] \langle F(\bar{t}) F(\bar{t}') \rangle. \end{aligned} \quad (9)$$

The expectation value vanishes unless the random phases are identical, which requires $|\bar{t} - \bar{t}'| < \tau_a$, so that

$$\langle F(\bar{t})F(\bar{t}')\rangle = \frac{1}{2}\langle A^2\rangle \cos\left[\omega_0(\bar{t}-\bar{t}')\right]\Theta(\tau_a - |\bar{t}-\bar{t}'|), \quad (10)$$

in terms of the step function $\Theta$. (Here, we have also used that $\varphi$ and $\mathbf{k}$ are uncorrelated.) The remaining expectation value can be determined by averaging over the incident direction of the axion, yielding

$$\langle A^2\rangle \simeq (2M_0 a_0 \omega_0)^2 \begin{cases} (g_N \omega_0 v)^2/3, \\ (g_d E^*)^2. \end{cases} \quad (11)$$

At short times ($t, t' \ll \tau_a$) where the axion is continuous, we have [cf. Eq. (8)],

$$C(t,t') = \frac{\langle A^2\rangle T_2^2}{8\omega_0^2}\cos[\omega_0(t-t')] \times (1 - e^{-t/T_2})(1 - e^{-t'/T_2}). \quad (12)$$

At longer times, the stochastic fluctuations in the axion associated with $\tau_a$ must be accounted for. Combining Eqs. (9) and (10), for $t, t' \gg \tau_a$ we can evaluate the integral by rotating coordinates to $\bar{t} \pm \bar{t}'$, yielding

$$C(t,t') = \frac{\langle A^2\rangle T_2 \tau_a}{16\omega_0^2}\cos[\omega_0(t-t')] \times e^{-(t+t')/T_2}(e^{2\ \min(t,t')/T_2} - 1). \quad (13)$$

Equations (12) and (13) allow us to infer the growth of the magnetization in the presence of a finite $\tau_a$, as $C(t,t) = \langle M_x^2(t)\rangle$. First, for $t \gg T_2$, we see that the growth saturates even with a finite coherence time in the driving force, implying saturation occurs in this limit regardless of the size of $\tau_a$. For $t \ll T_2$, however, the behaviors differ,

$$\lim_{t \ll T_2}\langle M_x^2(t)\rangle = \frac{\langle A^2\rangle}{8\omega_0^2}\begin{cases} t^2 & t \ll \tau_a, \\ \tau_a t & t \gg \tau_a. \end{cases} \quad (14)$$

The first result, that the amplitude of the magnetization grows linearly with time for $t \ll \tau_a, T_2$, is consistent with Eq. (8). However, for $\tau_a < t < T_2$, we see that the amplitude continues to grow, leading to an ever-increasing size, albeit as $\sqrt{t}$. Intuitively, this transition in behavior can be understood as the magnetization executing a random walk. For $t > \tau_a$, $M_x(t)$ in Eq. (6) is now a sum of contributions from the axion field at different coherence times, all of which are out of phase. The sum is analogous to a 2D random walk with steps of length $\tau_a$ (given the growth for $t < \tau_a$), and with a number of steps $t/\tau_a$, so that we expect $|M_x(t)| \propto \sqrt{t\tau_a}$, exactly as found (cf. Ref. [50]). In Fig. 1 (left), we show the growth of the magnetization for various axion masses, computed directly from Eq. (9). The three regimes ($t < \tau_a$, $\tau_a < t < T_2$, $T_2 < t$) can be clearly observed.

To compute the experimental sensitivity to a highly coherent axion signal, it is convenient to move to the frequency domain. We imagine a dataset $\{M_n = M_x(n\Delta t)\}$

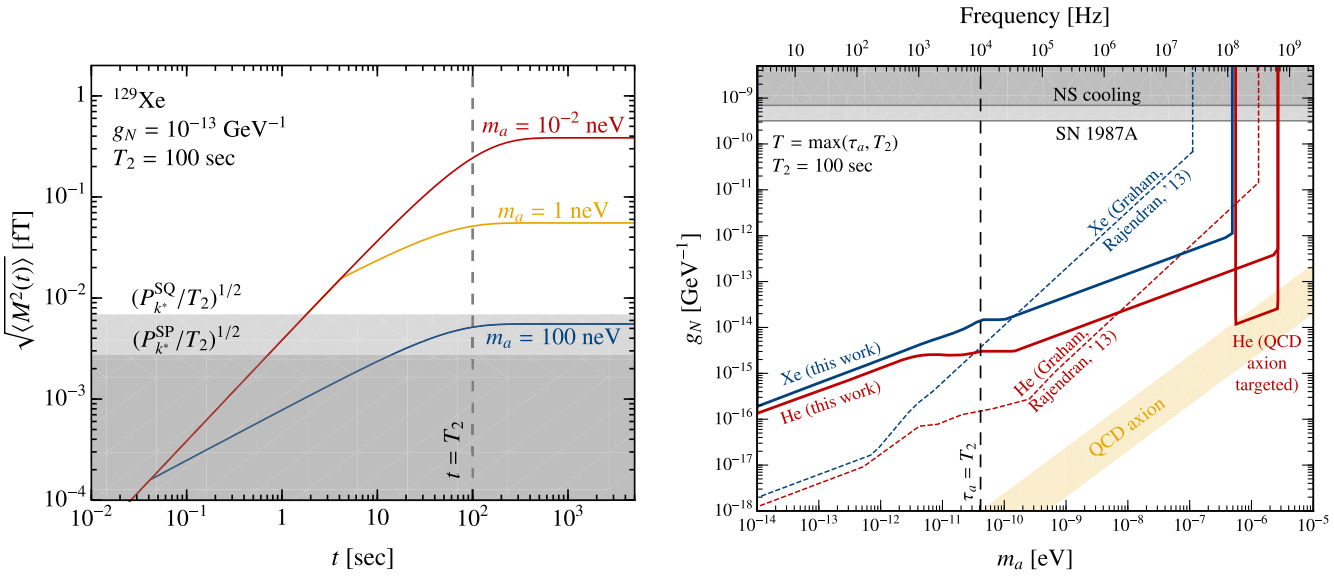


FIG. 1. Projections for the sensitivity of a prototypical spin-precession experiment to the magnetic dipole moment operator, $g_N(\partial_\mu a)\bar{N}\gamma^\mu\gamma_5 N$. Left: The axion-induced growth of the magnetization determined from the Bloch equations. At short times the magnetization grows $\propto t$, saturating at $T_2$. If $\tau_a < T_2$, the amplitude grows $\propto \sqrt{t}$ for $\tau_a < t < T_2$. The magnitudes are compared to those from a SQUID and spin-projection noise, evaluated at $k^* \equiv \omega_0 T/2\pi$, and assuming an integration time $T = T_2$. Right: Projected sensitivity to $g_N$ (solid) in comparison to previous projections of Ref. [12] (dashed), for an almost identical scan strategy. Strengthened sensitivity for $m_a \gg 2\pi/v^2 T_2$ arises primarily due to the signal growth we account for when $\tau_a < t < T_2$, whereas the suppression at lower masses arises partially from a refined estimate of the spin-projection noise. Blue and red lines correspond to xenon and helium targets, and for the latter we label a "QCD axion targeted" for the results that could be obtained with negligible spin-projection noise and five years of integration time.

of measurements of the magnetization collected at a frequency $1/\Delta t$, for an integration time $T = N\Delta t$. We can then compute the power spectral density (PSD) as [51],

$$P_k = \frac{\Delta t^2}{T}\langle|\tilde{M}_k|^2\rangle, \qquad \tilde{M}_k \equiv \sum_{n=0}^{N-1} e^{-i2\pi kn/N} M_n. \tag{15}$$

We can compute the PSD exactly for arbitrary $T$, $T_2$, and $\tau_a$ [52]. The result is particularly simple for $T \gg T_2$, taking the form

$$P_k^a \simeq \frac{\langle A^2\rangle T_2^2}{16\omega_0^2}\begin{cases} \frac{4}{\Delta\omega_k^2 T}\sin^2[\frac{1}{2}\Delta\omega_k T] & T \ll \tau_a, \\ \frac{\tau_a}{1+\Delta\omega_k^2 T_2^2} & T \gg \tau_a, \end{cases} \tag{16}$$

with $\Delta\omega_k \equiv 2\pi k/T - \omega_0$. Because of the resonant response of the sample, the signal peaks for $\Delta\omega_k \simeq 0$. For $T_2 \ll T \ll \tau_a$, the signal falls dominantly in a single $k$ bin, or, exactly, if $\omega_0 T/2\pi \in \mathbb{N}$. Once $T > \tau_a, T_2$, the signal becomes resolved into multiple bins. This will impact the signal-to-noise scaling, as we will discuss after considering the relevant background contributions.

*Noise sources.*—The axion signal must be detected on top of three relevant Gaussian background contributions: thermal noise, SQUID noise, and spin-projection noise [54]. Thermal noise arises in the readout circuit and can be suppressed by cooling the apparatus, and we assume this can be done sufficiently for this noise source to be neglected (for details, see Ref. [23]). The transverse magnetic field, related to the transverse magnetization by an $\mathcal{O}(1)$ factor which we take to be unity (see Ref. [47]), is read out using a SQUID. This magnetometer noise is frequency independent for $f \gtrsim 10$ Hz [56,57] and can be modeled as,

$$C_{\rm SQ}(t,t') = \delta(t-t')\frac{1}{A_{\rm eff}^2}P_{\Phi\Phi}^{\rm SQ} \Rightarrow P_k^{\rm SQ} = \frac{1}{A_{\rm eff}^2}P_{\Phi\Phi}^{\rm SQ}, \tag{17}$$

where by default, we take $P_{\Phi\Phi}^{\rm SQ} \simeq (\mu\Phi_0)^2/\text{Hz}$, with $\Phi_0$ the magnetic flux quantum, and $A_{\rm eff}$ is the effective area of the sample sensed by a pickup loop, which we take to be $\simeq 0.3$ cm$^2$, following Ref. [13].

The final background source we consider is spin-projection noise, which originates directly from the quantum nature of the nuclear spins in the sample [58]. We can determine its magnitude from the autocorrelation function. Consider two successive measurements of the spin operator along the $\hat{\mathbf{x}}$ direction, $S_x$, taken at $t$ and then $t'$. The operators are related through the time evolution operator, $\mathcal{U}(t) = \exp(i\omega_0 S_z t)$, $S_x(t') = \mathcal{U}^\dagger(t'-t)S_x(t)\mathcal{U}(t'-t)$. The magnetization can be determined from the sum over all nuclear spins, and assuming the sample is hyperpolarized (i.e., unit polarization fraction) we obtain,

$$\begin{aligned} C_{\rm SP}(t,t') &= \frac{\gamma^2}{2V^2}e^{-|t-t'|/T_2}\sum_i \langle S_x^{(i)}(t)S_x^{(i)}(t')\rangle + \text{H.c.} \\ &= \frac{\gamma^2 nJ}{2V}e^{-|t-t'|/T_2}\cos[\omega_0(t-t')], \end{aligned} \tag{18}$$

where $J$ is the nuclear spin, $n$ is the number density of spins, and $V$ is the volume of the sample. The exponential factor is included to account for transverse-spin relaxation, and for further details, see Ref. [47]. Equation (18) exhibits a $V^{-1}$ scaling, which suggests that for a large enough sample, this noise source can be suppressed. The corresponding PSD for $t, t' \gg T_2$ is given by

$$P_k^{\rm SP} = \frac{\gamma^2 nJ}{2V}\frac{T_2}{1+\Delta\omega_k^2 T_2^2}. \tag{19}$$

This result determines the spin-projection noise for an arbitrary $J$, assuming a hyperpolarized sample.

*Experimental sensitivity.*—We now combine the above results to forecast the expected sensitivity to an axion-induced signal. We use the signal PSD in the $\tau_a \gg T$ and $\tau_a \ll T$ limits and compare it to the background PSD, using all $k$-bins and the likelihood framework presented in [47] (employing the formalism of Ref. [50] and inserting the Asimov dataset [59]). Above the transition region of $\tau_a = T$, we interpolate between the two regimes with a horizontal line. In principle, one could extend our analysis to handle the intermediate regime. Detailed projections require us to specify explicit experimental parameters. Even before this, we can determine the sensitivity scaling with integration time, which varies depending on the hierarchy between $\tau_a$, $T_2$, and $T$. Specifically,

$$\begin{aligned} T \ll \tau_a, T_2 &\Rightarrow g \propto T^{-3/2} \\ \tau_a \ll T \ll T_2 &\Rightarrow g \propto T^{-1} \\ T_2 \ll T \ll \tau_a &\Rightarrow g \propto T^{-1/2} \\ \tau_a, T_2 \ll T &\Rightarrow g \propto T^{-1/4}, \end{aligned} \tag{20}$$

where $g = g_N, g_d$. The growth becomes slowest once $T$ is the largest timescale, and the signal is resolved into multiple bins. These scalings are derived in [47], however, they arise from comparing the growth of the signal and background. For instance, for $T_2 \ll T \ll \tau_a$, where the signal is dominantly in a single bin, $k^* \equiv \omega^0 T/2\pi$, we see that $P_{k^*}^a \propto T$ from Eq. (16), whereas $P_{k^*}^{\rm SQ}$ and $P_{k^*}^{\rm SP}$ are independent of $T$. Estimating sensitivity by matching the signal to the background, we find the limit scales as $g \propto T^{-1/2}$.

To provide quantitative projections, we match the parameters specified in the CASPEr papers [13,24], focusing on the magnetic dipole operator. The accessible Larmor frequencies set the mass range we consider, and we take $10^{-14}$ eV $< \omega_0 < \gamma B_{\rm max}$, with $B_{\rm max}$ the maximum magnetic field. We fix $T_2 = 100$ sec and for each mass, adopt a variable integration time, $T = \max[\tau_a, T_2]$, to ensure we always run until the $T^{-1/4}$ growth sets in from Eq. (20). This implies that the signal, and therefore the likelihood, remains dominated by a single frequency bin. To ensure

each mass is covered only once, resonant frequencies are adjusted by $2\pi \max[\tau_a^{-1}, T_2^{-1}]$.

We consider two different spin-1/2 samples, and both assumed to be hyperpolarized. The first consists of pure xenon-129, which has a nuclear magnetic moment of 0.78 $\mu_N$ and a nuclear spin density of $1.3 \times 10^{22}$ cm$^{-3}$, and we assume $B_{\max} = 10$ T. The second is a more optimistic projection using helium-3—$\mu = 2.12\ \mu_N$ and $n = 2.8 \times 10^{22}$ cm$^{-3}$—and $B_{\max} = 20$ T, as well as assuming the SQUID noise can be decreased by two orders of magnitude below that discussed around Eq. (17). As shown in [47], to cover the full mass range, these two experiments would require a total integration time of 56.1 and 61.5 yr, respectively.

Our results are shown in Fig. 1 (right), and contrasted with the projections of Ref. [12]. The discrepancy has at least three sources: (i) the additional growth of the signal we have accounted for when $\tau_a < T < T_2$, see Eq. (14); (ii) a different treatment of the spin-projection noise; and (iii) a different calculation of the Larmor frequency given $B_{\max}$ [60]. For the spin-projection noise, we compute the value for each $k$ with Eq. (19)—recall the signal is dominantly peaked in a single bin—rather than integrating a result over a range of frequencies near $\omega_0$, as in Eq. (A2) in Ref. [13]. Further discussion is provided in [47], where we also contrast our results for the electric dipole operator. As a final benchmark, in Fig. 1, we also show the helium-3 sensitivity assuming that spin-projection noise could be evaded, and the mass range is set by assuming five years of integration time. This benchmark cuts into the QCD axion parameter space, illustrated by the yellow band [61].

*Discussion.*—In this Letter we have derived the axion-induced signal in spin-precession experiments. These instruments remain one of the most promising paths to measuring axion-induced magnetic and electric dipoles, and our calculations demonstrate that their sensitivity is significantly different to what has previously been estimated. Arguably our most important finding is the enhanced detection prospects for the QCD axion at high masses, a result which arises from the continued growth of the axion-induced signal when integrating beyond the axion coherence time [62]. Our findings have broader implications. To name one, they demonstrate that signals that are less coherent than dark matter—for instance, a cosmic axion background [63]—are more detectable with spin-precession instruments than may otherwise have been concluded [64].

Our work benefited from conversations with Hendrik Bekker, Yonatan Kahn, Alexander Sushkov, and Arne Wickenbrock. Further, we thank the anonymous referee for useful feedback. J. M. L. is supported by the Deutsche Forschungsgemeinschaft under Germany's Excellence Strategy—EXC 2121 "Quantum Universe"—390833306. The research of J. D. and S. G. is supported in part by NSF CAREER Grant No. PHY-1915852 and in part by the U.S. Department of Energy Grant No. DE-SC0023093. Part of this work was performed at the Aspen Center for Physics, which is supported by National Science Foundation Grant No. PHY-1607611.

[1] R. Peccei and H. R. Quinn, *CP* Conservation in the Presence of Instantons, Phys. Rev. Lett. **38**, 1440 (1977).
[2] R. Peccei and H. R. Quinn, Constraints imposed by *CP* conservation in the presence of instantons, Phys. Rev. D **16**, 1791 (1977).
[3] S. Weinberg, A New Light Boson?, Phys. Rev. Lett. **40**, 223 (1978).
[4] F. Wilczek, Problem of Strong *P* and *T* Invariance in the Presence of Instantons, Phys. Rev. Lett. **40**, 279 (1978).
[5] P. Svrcek and E. Witten, Axions in string theory, J. High Energy Phys. 06 (2006) 051.
[6] A. Arvanitaki, S. Dimopoulos, S. Dubovsky, N. Kaloper, and J. March-Russell, String axiverse, Phys. Rev. D **81**, 123530 (2010).
[7] J. Halverson, C. Long, B. Nelson, and G. Salinas, Towards string theory expectations for photon couplings to axionlike particles, Phys. Rev. D **100**, 106010 (2019).
[8] L. Abbott and P. Sikivie, A cosmological bound on the invisible axion, Phys. Lett. **120B**, 133 (1983).
[9] J. Preskill, M. B. Wise, and F. Wilczek, Cosmology of the invisible axion, Phys. Lett. **120B**, 127 (1983).
[10] M. Dine and W. Fischler, The not so harmless axion, Phys. Lett. **120B**, 137 (1983).
[11] M. Pospelov and A. Ritz, Theta vacua, QCD sum rules, and the neutron electric dipole moment, Nucl. Phys. **573B**, 177 (2000).
[12] P. W. Graham and S. Rajendran, New observables for direct detection of axion dark matter, Phys. Rev. D **88**, 035023 (2013).
[13] D. Budker, P. W. Graham, M. Ledbetter, S. Rajendran, and A. Sushkov, Proposal for a Cosmic Axion Spin Precession Experiment (CASPEr), Phys. Rev. X **4**, 021030 (2014).
[14] Y. V. Stadnik and V. V. Flambaum, Axion-induced effects in atoms, molecules, and nuclei: Parity nonconservation, anapole moments, electric dipole moments, and spin-gravity and spin-axion momentum couplings, Phys. Rev. D **89**, 043522 (2014).
[15] C. Abel *et al.*, Search for Axionlike Dark Matter through Nuclear Spin Precession in Electric and Magnetic Fields, Phys. Rev. X **7**, 041034 (2017).
[16] T. Wang, D. F. Jackson Kimball, A. O. Sushkov, D. Aybas, J. W. Blanchard, G. Centers, S. R. O' Kelley, A. Wickenbrock, J. Fang, and D. Budker, Application of spin-exchange relaxation-free magnetometry to the cosmic axion spin precession experiment, Phys. Dark Universe **19**, 27 (2018).
[17] A. Garcon *et al.*, Constraints on bosonic dark matter from ultralow-field nuclear magnetic resonance, Sci. Adv. **5**, eaax4539 (2019).
[18] C. Smorra *et al.*, Direct limits on the interaction of antiprotons with axion-like dark matter, Nature (London) **575**, 310 (2019).

[19] T. S. Roussy *et al.*, Experimental Constraint on Axionlike Particles over Seven Orders of Magnitude in Mass, Phys. Rev. Lett. **126**, 171301 (2021).

[20] M. Jiang, H. Su, A. Garcon, X. Peng, and D. Budker, Search for axion-like dark matter with spin-based amplifiers, Nat. Phys. **17**, 1402 (2021).

[21] D. Aybas *et al.*, Search for Axionlike Dark Matter Using Solid-State Nuclear Magnetic Resonance, Phys. Rev. Lett. **126**, 141802 (2021).

[22] D. F. Jackson Kimball *et al.*, Overview of the cosmic axion spin precession experiment (CASPEr), Springer Proc. Phys. **245**, 105 (2020).

[23] D. Aybas, H. Bekker, J. W. Blanchard, D. Budker, G. P. Centers, N. L. Figueroa, A. V. Gramolin, D. F. J. Kimball, A. Wickenbrock, and A. O. Sushkov, Quantum sensitivity limits of nuclear magnetic resonance experiments searching for new fundamental physics, Quantum Sci. Technol. **6**, 034007 (2021).

[24] P. W. Graham and S. Rajendran, Axion dark matter detection with cold molecules, Phys. Rev. D **84**, 055013 (2011).

[25] P. Sikivie, Axion Dark Matter Detection using Atomic Transitions, Phys. Rev. Lett. **113**, 201301 (2014); **125**, 029901(E) (2020).

[26] P. W. Graham, D. E. Kaplan, J. Mardon, S. Rajendran, W. A. Terrano, L. Trahms, and T. Wilkason, Spin precession experiments for light axionic dark matter, Phys. Rev. D **97**, 055006 (2018).

[27] S. P. Chang, S. Haciomeroglu, O. Kim, S. Lee, S. Park, and Y. K. Semertzidis, Axionlike dark matter search using the storage ring EDM method, Phys. Rev. D **99**, 083002 (2019).

[28] S. Chang, O. Kim, Y. Semertzidis, S. Haciomeroglu, S. Lee, and S. Park, Axion searches with the storage ring EDM method, Proc. Sci., ICHEP2018 (**2019**) 842.

[29] T. Wu *et al.*, Search for Axionlike Dark Matter with a Liquid-State Nuclear Spin Comagnetometer, Phys. Rev. Lett. **122**, 191302 (2019).

[30] W. A. Terrano, E. G. Adelberger, C. A. Hagedorn, and B. R. Heckel, Constraints on Axionlike Dark Matter with Masses Down to $10^{-23}$ eV/c$^2$, Phys. Rev. Lett. **122**, 231301 (2019).

[31] I. M. Bloch, Y. Hochberg, E. Kuflik, and T. Volansky, Axion-like Relics: New constraints from old comagnetometer data, J. High Energy Phys. 01 (2020) 167.

[32] Q. Yang, Probe dark matter axions using the hyperfine structure splitting of hydrogen atoms, arXiv:1912.11472.

[33] F. Abusaif *et al.*, Storage ring to search for electric dipole moments of charged particles—feasibility study, arXiv:1912.07881.

[34] V. V. Flambaum, D. Budker, and A. Wickenbrock, Oscillating nuclear electric dipole moments inside atoms, arXiv:1909.04970.

[35] E. Stephenson (JEDI Collaboration), A search for axion-like particles with a horizontally polarized beam in a storage ring, Proc. Sci., PSTP2019 (**2020**) 018.

[36] A. V. Gramolin, D. Aybas, D. Johnson, J. Adam, and A. O. Sushkov, Search for axion-like dark matter with ferromagnets, Nat. Phys. **17**, 79 (2021).

[37] P. W. Graham, S. Hacıömeroğlu, D. E. Kaplan, Z. Omarov, S. Rajendran, and Y. K. Semertzidis, Storage ring probes of dark matter and dark energy, Phys. Rev. D **103**, 055010 (2021).

[38] K. Gaul, M. G. Kozlov, T. A. Isaev, and R. Berger, Chiral Molecules as Sensitive Probes for Direct Detection of P-Odd Cosmic Fields, Phys. Rev. Lett. **125**, 123004 (2020).

[39] A. Arvanitaki, A. Madden, and K. Van Tilburg, The piezoaxionic effect, arXiv:2112.11466.

[40] O. Kim and Y. K. Semertzidis, New method of probing an oscillating EDM induced by axionlike dark matter using an rf Wien filter in storage rings, Phys. Rev. D **104**, 096006 (2021).

[41] C. Gao, W. Halperin, Y. Kahn, M. Nguyen, J. Schütte-Engel, and J. W. Scott, Axion Wind Detection with the Homogeneous Precession Domain of Superfluid Helium-3, Phys. Rev. Lett. **129**, 211801 (2022).

[42] A. Berlin and K. Zhou, Discovering QCD-coupled axion dark matter with polarization haloscopes, arXiv:2209.12901.

[43] M. Lisanti, M. Moschella, and W. Terrano, Stochastic properties of ultralight scalar field gradients, Phys. Rev. D **104**, 055037 (2021).

[44] J. Lee, M. Lisanti, W. A. Terrano, and M. Romalis, Laboratory Constraints on the Neutron-Spin Coupling of feV-Scale Axions, Phys. Rev. X **13**, 011050 (2023).

[45] This is an excellent approximation. If we take $T_2, \tau_a \to \infty$, then $M_x(t) \sim g_N v\sqrt{2\rho_{\rm DM}} M_0 \sin(\omega_0 t) t$ for the MD interaction, see Eq. (8). This suggests that with enough time an infinite magnetization can be generated, which is inconsistent with the finite number of spins in the system. Terms higher order in $g_N$ prevent this from occurring. We can estimate when they must enter by determining when $M_x(t) \sim M_0$. Setting $g_N$ to the largest allowed value (set by the SN 1987A bound), we find $t \sim 30$ years, dramatically larger than $T_1$ for any sample we consider, which represents the longest time we can interrogate the sample for. Including a finite $T_2$ or $\tau_a$ only strengthens this conclusion.

[46] The solution in Eq. (6) is for the Bloch equation before terms of $\mathcal{O}(1/\omega_0 T_2)$ are dropped; cf. Eq. (5).

[47] See Supplemental Material at http://link.aps.org/supplemental/10.1103/PhysRevLett.130.181801 for further details.

[48] The coherence time is a measure of how long the axion field can be approximated as a perfectly coherent driving force, or in the frequency domain how long of a measurement is required to resolve the intrinsic width of the axion. It is an approximate notion, as the transition from perfectly coherent to incoherent happens gradually near $t \sim 2\pi/m_a v^2$, not exactly at $\tau_a$. For further discussion of the coherence time, see, for instance, Ref. [49].

[49] J. W. Foster, Y. Kahn, R. Nguyen, N. L. Rodd, and B. R. Safdi, Dark matter interferometry, Phys. Rev. D **103**, 076018 (2021).

[50] J. W. Foster, N. L. Rodd, and B. R. Safdi, Revealing the dark matter halo with axion direct detection, Phys. Rev. D **97**, 123006 (2018).

[51] In Eq. (15) we specify the expectation value of the PSD, rather than the PSD itself. Given a single experimental dataset, the average PSD cannot be computed, and it will vary between realizations as the axion field which gave rise to it is stochastic. Nevertheless, our goal is to determine what value we expect to generate, and so we will compute

the expected PSD throughout. A more careful distinction is provided in [47].
[52] This is discussed in detail in [47]. Also see Refs. [41,43,44,53] for related considerations.
[53] A. V. Gramolin, A. Wickenbrock, D. Aybas, H. Bekker, D. Budker, G. P. Centers, N. L. Figueroa, D. F. J. Kimball, and A. O. Sushkov, Spectral signatures of axionlike dark matter, Phys. Rev. D **105**, 035029 (2022).
[54] In both the fluctuating phase and plane wave models, the axion field itself forms a Gaussian random field, and hence one can show so too does any linear functional of the axion (see, e.g., Ref. [55], Appendix E).
[55] S. Weinberg, *Cosmology* (Oxford University Press, Oxford, 2008).
[56] S. M. Anton, J. S. Birenbaum, S. R. O'Kelley, V. Bolkhovsky, D. A. Braje, G. Fitch, M. Neeley, G. C. Hilton, H.-M. Cho, K. D. Irwin, F. C. Wellstood, W. D. Oliver, A. Shnirman, and J. Clarke, Magnetic Flux Noise in dc Squids: Temperature and Geometry Dependence, Phys. Rev. Lett. **110**, 147002 (2013).
[57] Y. Kahn, B. R. Safdi, and J. Thaler, Broadband and Resonant Approaches to Axion Dark Matter Detection, Phys. Rev. Lett. **117**, 141801 (2016).
[58] M. Braun and J. König, Faraday-rotation fluctuation spectroscopy with static and oscillating magnetic fields, Phys. Rev. B **75**, 085310 (2007).
[59] G. Cowan, K. Cranmer, E. Gross, and O. Vitells, Asymptotic formulae for likelihood-based tests of new physics, Eur. Phys. J. C **71**, 1554 (2011); **73**, 2501(E) (2013).
[60] For helium our result is exactly a factor of two larger, whereas for xenon the difference is slightly larger than a factor of 4. For xenon, this difference is attributed to the use of a combination of isotopes, whereas we considered a pure sample of xenon-129.
[61] The band is defined as the region bounded from below by the KSVZ axion model and from above by the DFSZ model with the down-type Higgs doublet vacuum expectation value set to zero. (Note that the full range of DFSZ Higgs' vacuum expectation values allows the QCD axion parameter space to fill the entire lower right corner of Fig. 1.)
[62] In light of our results, one may wonder if its possible to build an experiment using an element that carries a larger gyromagnetic ratio than helium-3 to increase the maximum testable axion mass and improve the coverage of the QCD axion line. Surveying all measured gyromagnetic moments of nuclear isotopes, the only element with a substantially larger value is thallium-200, although since it carries a half-life of $\sim$1 day it does not appear viable. Tritium, atomic hydrogen, and fluorine-19 have larger gyromagnetic ratios than helium-3, but by less than 40%.
[63] J. A. Dror, H. Murayama, and N. L. Rodd, Cosmic axion background, Phys. Rev. D **103**, 115004 (2021).
[64] J. A. Dror, S. Gori, J. M. Leedom, and N. L. Rodd (to be published).